

# A persistent-homology-based Bayesian prior to identify Robin coefficient in parabolic problems

Xiaomei Yang,<sup>1</sup> Jiaying Jia<sup>2</sup>

## Abstract

We adopt a Bayesian inference approach with persistent-homology-based prior to estimate a temporally dependent Robin coefficient arising in the analysis of convective heat transfer. And we also discuss the use of a hierarchical Bayesian method for automatic selection of the regularization parameter. Numerical results demonstrate that the PH prior shows consistent improvement compared to the Gaussian and the total variation prior.

**Keywords:** Robin inverse problem, persistent-homology-based prior, Bayesian inference approach, Hierarchical Bayesian model.

## 1 Introduction

The Robin coefficient characterizes the intensity of heat exchange in convective heat transfer and reflects the physical behavior near boundaries[1, 2, 3, 4]. In this paper, we consider the following initial-boundary value problem for the parabolic equation:

$$\begin{cases} \frac{\partial u}{\partial t}(x, t) - \frac{\partial u}{\partial x}(\alpha(x) \frac{\partial u}{\partial x}(x, t)) = f(x, t) & \text{in } Q, \\ \alpha(x) \frac{\partial u}{\partial x}(x, t) = h_0(t) & \text{on } \Sigma_c, \\ \alpha(x) \frac{\partial u}{\partial x}(x, t) + \gamma(t)u(x, t) = h_1(t) & \text{on } \Sigma_i, \\ u(x, 0) = g(x) & \text{in } \Omega \end{cases} \quad (1)$$

where  $\alpha(x)$  is the known thermal conductivity,  $\gamma(t)$  is the Robin coefficient to be identified, and  $f$  is the source term. Here,  $T > 0$  is an arbitrarily given time,  $h_0(t)$ ,  $h_1(t)$ , and  $g(x)$  are known functions, and  $u$  represents the temperature. The boundary  $\Gamma$  consists of two disjoint parts  $\Gamma = \Gamma_i \cup \Gamma_c$ , where both  $\Gamma_i$  and  $\Gamma_c$  are unions of several  $(d - 1)$ -dimensional polyhedral regions. Here,  $\Gamma_i$  and  $\Gamma_c$  correspond to the inaccessible and accessible parts of the boundary in experiments, respectively. The inverse problem is to estimate the spatially-andtemporally dependent Robin coefficient  $\gamma(x, t)$  on the boundary  $\Gamma_i$ . To investigate the time-space dependent problem, we define the space-time domains  $Q$  and  $\Sigma_i$  as follows:

$$Q = (0, T) \times \Omega \quad \text{and} \quad \Sigma_i = (0, T) \times \Gamma_i$$

The domain  $\Sigma_c$  is defined analogously. We collect the observational data of the solution  $Y$  to (1) by:

$$Y = u(x, t) + \eta(x, t), \quad (2)$$

where  $\eta$  denotes the measurement noise. Our aim is to estimate the potential function  $\gamma(t)$  from the noisy observation  $Y$ .

For the inverse problem of the Robin coefficient, numerous works have established theoretical results, including existence, uniqueness, and stability of solutions [5, 6, 7, 8, 9, 10, 11]. Apart from theoretical analysis, many numerical methods have been proposed for identifying the Robin coefficient. Onyango et al. [12] used the boundary element method to handle coefficient inversion. F.Yang et al. [13] applied the conjugate-gradient approach to estimate the Robin problem. W.Fang and S.Zeng [14] combined boundary integral equations method with regularization techniques to reconstruct spatially dependent coefficients. B.Jin and X.Lu [11] solved space-time dependent Robin coefficients with gradient-based optimization under Tikhonov regularization. da Silva et al. [15] combined the method of fundamental

<sup>1</sup>Author1 title, Author1 institution, Author1 institution country, Author1 email.

<sup>2</sup>Author2 title, Author2 institution, Author2 institution country, Author2 email.

---

solutions with a sequential importance resampling particle filter algorithm to estimate a time-dependent heat transfer coefficient.

In recent years, the Bayesian framework has gained increasing attention in the identification of Robin coefficients. Bayesian inference is well suited to quantify uncertainty and to handle complex data. Many prior models have been proposed. Among them, [16, 17, 18, 19] use the Markov random field (MRF); Rasmussen et al. [20] employ Matérn and squared-exponential Gaussian priors; and Z. Yao et al. [21] propose a TV–Gaussian hybrid prior that can capture sharp jumps in the target. In addition, [16, 17, 19] adopt a hierarchical Bayesian method to select the regularization parameter automatically. In addition, this paper adopts a hierarchical Bayesian approach to select the regularization parameter automatically.

Building on the existing studies, we adopt a prior constructed on the topological tool of persistent homology (PH prior). This prior was originally proposed in [22] for Bayesian inversion of potential coefficients, but to the best of our knowledge, it has not yet been applied to the identification of Robin coefficients. And [22] did not provide a concrete strategy for selecting the regularization parameter  $\lambda$ . In this paper, we address this issue by incorporating a hierarchical Bayesian framework to infer  $\lambda$  from the data. By quantifying and encoding the topological features of the unknown function, the PH prior effectively preserves both global structures and local discontinuities during the inversion process. Compared with Gaussian priors, the PH prior shows better performance in handling target functions with sharp discontinuities or complex structures; at the same time, it preserves richer topological information than the TV prior.

The remainder of this paper is organized as follows. Section 2 describes fundamental ideas of Bayesian inference with an emphasis on PH prior and hierarchical Bayesian models. Section 3 provides numerical examples to validate the effectiveness of the proposed approach. Section 4 concludes the paper.

## 2 The Bayesian approach with the PH-Gaussian prior

In this section, we describe the Bayesian formulation used for identifying the Robin coefficient with the PH–Gaussian prior. We first outline the basic components of Bayesian inference, including the PH–Gaussian prior. We then introduce the hierarchical Bayesian framework used to determine the regularization parameter  $\lambda$ . Finally, we describe the numerical sampling method employed to explore the posterior state space.

### 2.1 Bayesian inference fundamentals

In the Bayesian statistical inversion framework, all variables are modeled as random variables. Unlike deterministic inversion, the aim is to estimate the posterior probability density of the unknown parameter  $\gamma(t)$  given data  $Y$ . By Bayes’ theorem, the posterior is determined by the prior and the likelihood:

$$\pi(\gamma|Y) \propto \pi(Y|\gamma)\pi(\gamma), \quad (3)$$

where  $\pi(Y|\gamma)$  is the likelihood function and  $\pi(\gamma)$  is the prior distribution.

Since the noise  $\eta$  follows a Gaussian distribution with mean 0 and covariance matrix  $\Sigma$ , the likelihood function can be written as:

$$\pi(Y|\gamma) \propto \exp(-\Phi(\gamma; Y)),$$

where:

$$\Phi(\gamma; Y) := \frac{1}{2}\|F(\gamma) - Y\|_{\Sigma}^2 = \frac{1}{2}\|\Sigma^{-1/2}(F(\gamma) - Y)\|_2^2.$$

This term quantifies the misfit between the model parameters and the observed data. A smaller value indicates a better fit. We assume the prior distribution is  $\mu_{\text{pr}}$  and the posterior distribution is  $\mu_{\text{post}}$ , given by the Radon–Nikodym derivative:

$$\frac{d\mu_{\text{post}}}{d\mu_{\text{pr}}}(\gamma) = \frac{1}{Z} \exp(-\Phi(\gamma; Y)),$$

where  $Z$  is a normalization constant ensuring the posterior measure is normalized to a probability distribution. The most widely used prior in Bayesian inverse problems is the Gaussian prior, i.e.,  $\mu_{\text{pr}} = \mu_0$ ,

---

where  $\mu_0 = N(0, C_0)$ . In practical terms, the Gaussian prior reflects our belief that the unknown parameter  $\gamma$  has a mean of 0 before any data is observed. The covariance  $C_0$  represents our assumption about the variability or uncertainty in  $\gamma$ .

Then we define the covariance operator  $C_0$  as an integral operator with a mean squared exponential:

$$C_0^{\exp} \iota = \int_{\Omega} \exp\left(-\frac{|x-y|^2}{2l^2}\right) \iota(y) dy$$

where  $d > 0$  is a length-scale parameter.

In order to capture nonsmooth features, we add extra constraints to the Gaussian prior and form a hybrid prior. The idea follows Yao et al. [21]: integrate modeling and constraints of different types within one framework to increase prior flexibility. This hybrid strategy improves the representation of complex systems, especially when both uncertainty and structural information are present.

In [21], the authors adopt hybrid priors and suppose

$$\frac{d\mu_{\text{pr}}}{d\mu_0}(\gamma) \propto \exp(-R(\gamma)),$$

instead of simply letting  $\mu_{\text{pr}} = \mu_0$ , where  $R(\gamma)$  represents additional prior information on  $\gamma$ . Thus, the Radon-Nikodym derivative of the posterior measure  $\mu_{\text{post}}$  with respect to  $\mu_0$  can be expressed as:

$$\frac{d\mu_{\text{post}}}{d\mu_0}(\gamma) \propto \exp(-\Phi(\gamma; u^n) - R(\gamma)),$$

When  $R(\gamma) = 0$ , this reduces to the form under the standard Gaussian prior.

In the numerical implementation, the domain  $\Omega$  is discretized into  $N_t + 1$  grid points, and the TV regularization term can be approximated as:

$$R_{\text{TV}} = \lambda \sum_{i=1}^{N_t} |\gamma_{i+1} - \gamma_i|, \quad (4)$$

Let  $\mathbf{X}$  be a partition of the interval  $a = x_0 < x_1 < \dots < x_N = b$ . The PH-Gaussian prior term is based on the concept of persistent distance, defined as:

$$\|\gamma\|_{\text{per}} = \|y\|_{\text{per}} = \|y|\mathbf{X}\|_{\text{per}} := \sum_{(x_k, x_l) \in P_1} |\gamma(x_l) - \gamma(x_k)| + \sum_{(x_k, x_l) \in P_2} |\gamma(x_l) - \gamma(x_k)|,$$

which sums the functional value distances of all persistent pairs in  $P_1$  and  $P_2$ . The persistent distance is composed of the sum of functional value distances between local extreme points of the function  $\gamma$ , describing the topological characteristics of  $u$ . Here, smaller distances  $|\gamma(x) - \gamma(\tilde{x})|$  (corresponding to short persistent pairs  $(x, \tilde{x})$ ) reflect noise-like oscillatory behavior, while larger distances  $|\gamma(x) - \gamma(\tilde{x})|$  characterize significant features of the function  $\gamma$ .

For the one-dimensional case, the prior distribution is defined as:

$$\frac{d\mu_{\text{pr}}}{d\mu_0}(\gamma) \propto \exp\left(-\sum_{(x_j, \tilde{x}_j) \in P(\gamma)} \alpha_j(\gamma) |\gamma(x_j) - \gamma(\tilde{x}_j)|\right),$$

where the weights  $\alpha_j = \alpha_j(\gamma) = \alpha(\gamma, x_j, \tilde{x}_j)$  depend on the persistence  $|\gamma(x_j) - \gamma(\tilde{x}_j)|$ : for smaller distances  $|\gamma(x_j) - \gamma(\tilde{x}_j)|$ ,  $\alpha_j$  should take larger values; for larger distances  $|\gamma(x_j) - \gamma(\tilde{x}_j)|$ ,  $\alpha_j$  should take smaller values. The regularization term  $R(\gamma)$  is expressed as:

$$R(\gamma) = \lambda \sum_{(x_j, \tilde{x}_j) \in P(\gamma)} \alpha_j(\gamma) |\gamma(x_j) - \gamma(\tilde{x}_j)|. \quad (5)$$

By appropriately selecting  $\alpha_j$ , the reconstructed function  $\gamma$  can effectively retain the key features of the original  $\mathbf{y} = (\gamma(x_j))_{j=0}^N$ . Therefore, we need to consider not only the local behavior of the function on the interval  $[x_l, x_{l+1}]$ , but also incorporate the structural information of the corresponding persistence

---

pairs. If prior knowledge about the hierarchical structure of the original signal (such as the hierarchy level of the chains) is available, it becomes possible to more accurately determine which persistence pairs represent significant features. Noise typically corresponds to high-order persistence pairs, while low-order pairs reflect important structures. Based on the hierarchical information of the chains, for any persistence pair  $(x_j, \tilde{x}_j) \in P(\gamma)$ , the weight can be set as:

$$\alpha_j(\gamma) = (k_j + 1)\tau \cdot \frac{1}{1 + \eta|\gamma(\tilde{x}_j) - \gamma(x_j)|},$$

where  $\tau > 1$ ,  $k_j = k(x_j, \tilde{x}_j)$  denotes the hierarchy level of the persistence pair  $(x_j, \tilde{x}_j)$  within the chain, and  $\eta > 0$  is a parameter that adjusts the sensitivity to functional value differences.

## 2.2 Hierarchical Bayesian models

To let the regularization level  $\lambda$  be chosen by the data, we treat  $\lambda$  as a random hyper-parameter and place a Gamma prior. This gives a hierarchical model. The hierarchical Bayesian posterior density is

$$p(\gamma, \lambda | Y) \propto p(Y | \gamma, \lambda) p(\gamma | \lambda) p(\lambda).$$

For the hyper-parameter, a conjugate prior is a standard choice. In (4)–(5) we use a Gamma prior for  $\lambda$ :

$$p(\lambda) \propto \lambda^{m_1-1} e^{-m_2\lambda}$$

Combining the above prior structure with the prior for  $\lambda$ , the hierarchical Bayesian posterior distribution can be computed as:

$$p(\gamma, \lambda | Y) \propto \exp\left(-\frac{1}{2\sigma^2}\|\mathbf{F}(\gamma) - Y\|_2^2\right) \exp\left(-\frac{1}{2}\|\gamma\|_E^2\right) \exp(-R(\gamma)) \lambda^{m_1-1} e^{-m_2\lambda}$$

and the full conditional distribution  $p(\lambda | \gamma, Y)$  can be given as

$$p(\lambda | \gamma, Y) \propto \lambda^{m_1-1} \exp(-(m_2\lambda + R(\gamma)))$$

## 2.3 Numerical exploration of the posterior state space

This paper employs the preconditioned Crank–Nicolson (PCN) and Gibbs algorithm to sample from the posterior distribution  $p(\gamma, \lambda | Y)$ , obtaining representative samples of the posterior parameters for further statistical analysis of the state space.

---

### Algorithm 1

- 1: **Initialization:** Set sample size  $N$ . Take  $\gamma^{(0)}, \lambda^{(0)}$ . Denote  $\varphi^{(0)} := \Phi(\gamma^{(0)}; Y) + \lambda R(\gamma^{(0)}) + \frac{1}{2}\|\gamma^{(0)}\|_E^2 - \log p(\lambda^{(0)})$
- 2: Propose a candidate sample  $\hat{\gamma}^{(n)} = \sqrt{1 - \beta^2}\gamma^{(n-1)} + \beta\xi$ , where  $\xi \sim \mathcal{N}(0, C_0)$ ;
- 3: Denote  $\hat{\varphi}^{(n)} := \Phi(\hat{\gamma}^{(n)}; Y) + \lambda R(\hat{\gamma}^{(n)}) + \frac{1}{2}\|\hat{\gamma}^{(n)}\|_E^2 - \log p(\lambda^{(n-1)})$ .
- 4: Compute the acceptance probability  $\alpha = \min\{1, \exp[-\hat{\varphi}^{(n)} + \varphi^{(n-1)}]\}$ .
- 5: Update  $\gamma^{(n)}$ : If  $\alpha > \theta$ , set  $\gamma^{(n)} = \hat{\gamma}^{(n)}$ ; else set  $\gamma^{(n)} = \gamma^{(n-1)}$ , where  $\theta \sim U(0, 1)$ .
- 6: Update  $\lambda^{(n)}$  via Gibbs sampling:  $\lambda^{(n)} \sim \Gamma(m_1, R(\gamma) + m_2)$
- 7: While  $n < N$ , repeat Steps 2–6.

---

In the aforementioned algorithm, the regularization term is given by  $R(\gamma) = \sum_{i=1}^{N_t} |\gamma_{i+1} - \gamma_i|$  for the TV–Gaussian prior and  $R(\gamma) = \sum_{(x_j, \tilde{x}_j) \in P(\gamma)} \alpha_j(\gamma) |\gamma(x_j) - \gamma(\tilde{x}_j)|$  for the PH–Gaussian prior. A burn-in phase is incorporated in the sampling procedure. We discard the first 30% of the initially generated samples as the burn-in period to minimize the influence of the initial distribution on stationary sampling. Finally, the mean of all post-burn-in samples is adopted as the posterior estimate of the parameter.

### 3 Numerical experiments

In this section, we consider three one-dimensional examples to assess the effectiveness of the PH-Gaussian prior for identifying the Robin coefficient. We conduct the inversion using three different priors: a Gaussian prior, a TV-Gaussian prior and a PH-Gaussian prior and compare the numerical results obtained under each prior. The spatial domain  $\Omega$  for the numerical examples is set to  $(0, 1)$  and the final time is fixed at  $T = 1$ . Temperature is measured on  $\Gamma_c = \{x = 0\}$ , while the time-dependent Robin coefficient  $\gamma(t)$  on  $\Gamma_i = \{x = 1\}$  is to be estimated. The spatial domain  $\Omega$  is discretized into 100 elements and the number of time steps is 200. For all experiments, the number of samples is set to  $N = 10^5$ . The chosen hyperparameters are  $m_1 = 50$  and  $m_2 = 0.1$  for Example 1 and Example 2, while  $m_1 = 200$  and  $m_2 = 0.1$  for Example 3. In all examples, the observations  $Y$  are generated as

$$Y(x_i) = F(\gamma)(x_i) + F(\gamma)(x_i)\varepsilon\omega, \quad i = 1, \dots, h$$

where the forward map is  $\mathbf{F} : \gamma \mapsto u(0, t; \gamma)$ . Here  $\varepsilon$  denotes the relative noise.  $\omega$  is a Gaussian random variable with mean 0 and standard deviation 1.

To evaluate the accuracy of the numerical inversion results  $\gamma(t)$ , this paper adopts the following relative error metric:

$$\text{error}(\gamma) = \frac{\sqrt{\sum_{i=1}^m (\gamma_i - \hat{\gamma}_i)^2}}{\sqrt{\sum_{i=1}^m (\gamma_i)^2}}$$

where  $\gamma_i$  and  $\hat{\gamma}_i$  represent the exact value and the inverted value at the discrete node  $t_i$ , respectively.

Example 1: The conductivity  $\alpha(x)$  is set as  $\alpha = 1$ , and the exact Robin coefficient  $\gamma^\dagger(t)$  is given by  $\gamma^\dagger(t) = 2 + \sin(2\pi t)$ . The boundary conditions, source term, and initial condition are specified such that the analytical solution to the direct problem (1) is given by  $u(x, t) = e^{2x} \sin(t)$ .

This test compares three methods: a Gaussian prior based on  $C_0^{\text{exp}}$ , a TV-Gaussian prior, and a PH-Gaussian prior. For the latter two priors, we also adopt the Gaussian prior based on  $C_0^{\text{exp}}$ . The parameters are  $l = 0.25$  and  $\delta = 0.1$  in  $C_0^{\text{exp}}$ , and  $\theta = 3$  and  $\beta = 0.001$  in the topological prior. The numerical results for Example 1 with 1% and 5% noise in the data are shown in Figure 1:

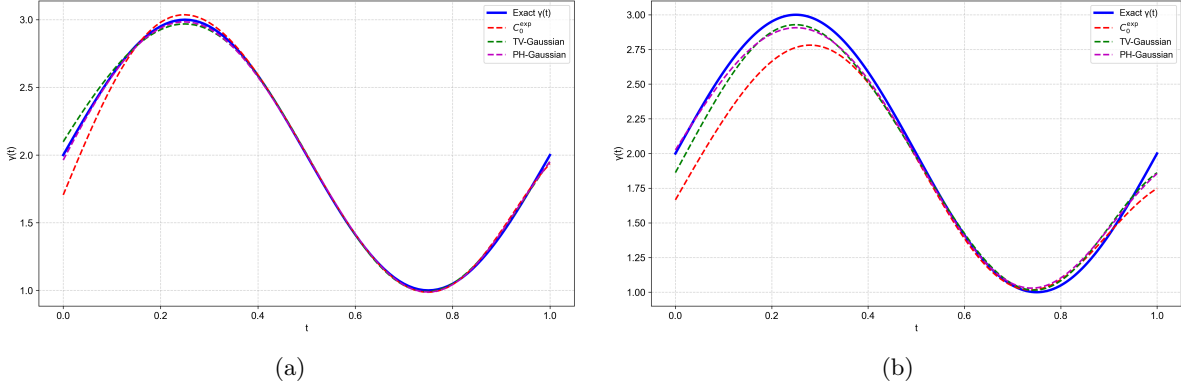


Figure 1: The numerical results for Example 1 with (a) 1% and (b) 5% noise added into the data.

As can be seen from Figure 1, in Example 1, the Gaussian prior, the TV Gaussian prior, and the PH Gaussian prior all deliver accurate reconstructions for the smooth target with 1% noise in the data. Among them, the TV Gaussian and PH Gaussian priors produce reconstructions that closely match the true solution.

Table 1 shows that all three priors achieve small relative errors for the smooth Example 1, indicating satisfactory reconstruction quality. In particular, the TV Gaussian and PH Gaussian priors yield slightly lower errors than the Gaussian prior.

The posterior densities of the parameter  $\lambda$  with 1% noise added into the data for the TV Gaussian and PH Gaussian priors are shown in Figure 2, and the corresponding posterior conditional means are listed in Table 1. The numerical results indicate that the automatically determined  $\lambda$  is close to optimal. Figure 3 presents the reconstruction obtained with the PH Gaussian prior; the vertical bars denote the

Table 1: Numerical results of Example 1 with different noise levels

$\epsilon$	Gaussian Prior		TV-Gaussian Prior		PH-Gaussian Prior	
	$\hat{\lambda}$	$e_r$	$\hat{\lambda}$	$e_r$	$\hat{\lambda}$	$e_r$
0.01	/	0.0315	12.61	0.0127	4.16	0.0064
0.03	/	0.0507	12.19	0.0190	4.28	0.0124
0.05	/	0.0840	12.72	0.0322	4.61	0.0261

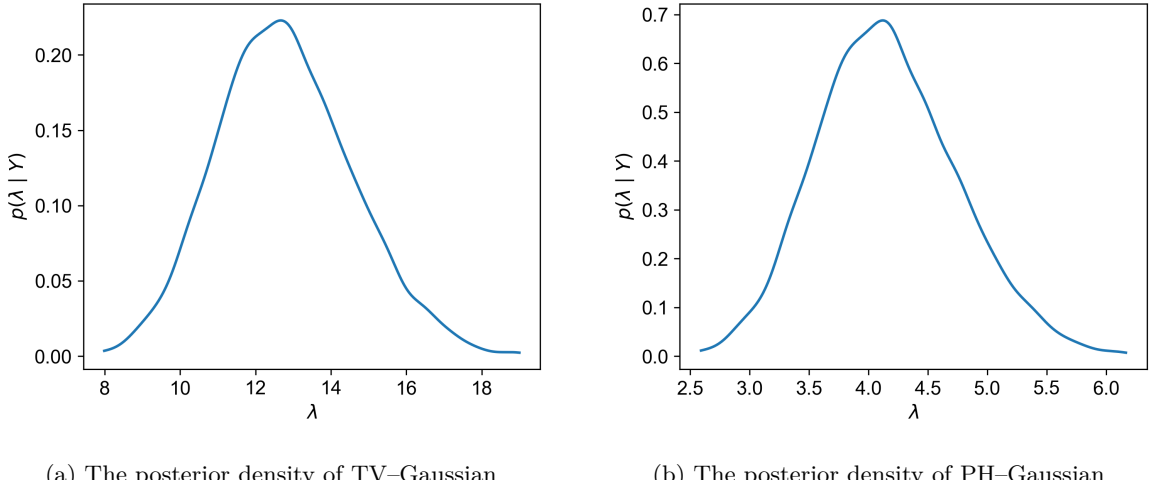


Figure 2: The posterior density of the scaling parameter  $\lambda$  for Example 1 with 1% noise added into the data.

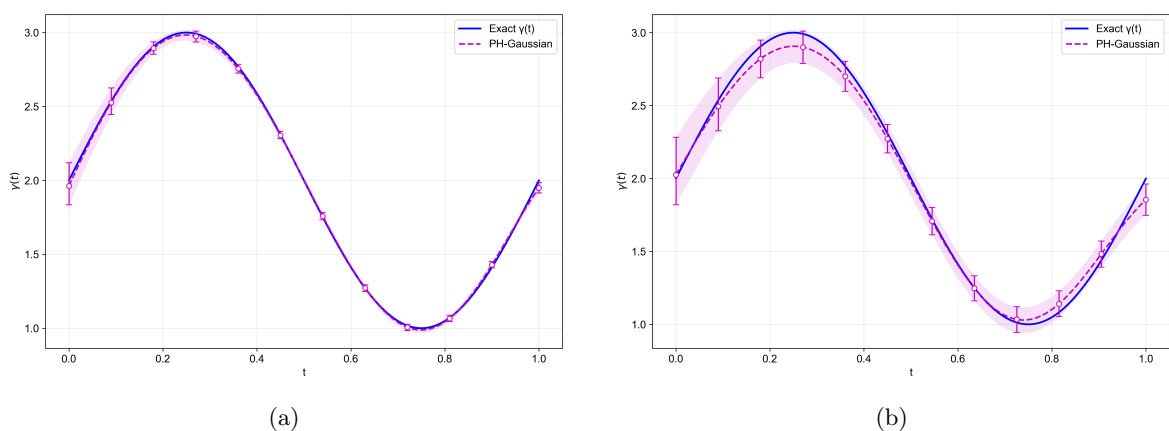


Figure 3: The numerical results for Example 1 with (a) 1% and (b) 5% noise added into the data.

95% credible interval, which quantifies the uncertainty of the mean. From this figure, the posterior conditional mean  $\gamma$  agrees very well with the exact solution.

Example 2. The conductivity  $\alpha(x)$  is set as  $\alpha(x) = 1$ , and the exact Robin coefficient  $\gamma^\dagger(t)$  is given by  $\gamma(t) = \begin{cases} 2t, & 0 \leq t \leq \frac{1}{2}, \\ 2(1-t), & \frac{1}{2} < t \leq 1. \end{cases}$ . The boundary conditions, source term, and initial condition are specified such that the analytical solution to the direct problem (1) is given by  $u(x, t) = (x+1)(t+1)$ .

In this example, we again test three priors. The prior parameters are  $l = 0.15$  and  $\delta = 0.1$  in  $C_0^{\text{exp}}$ , and  $\theta = 3$  and  $\beta = 0.001$  in the topological prior. The number of samples is  $N = 10^5$ . The numerical results for Example 2 with 1% and 5% noise in the data are shown in Figure 4:

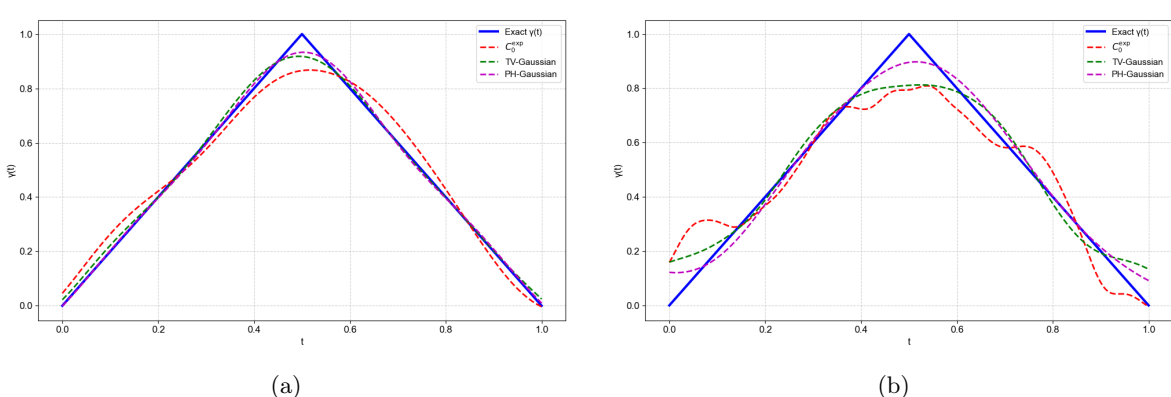


Figure 4: The numerical results for Example 2 with (a) 1% and (b) 5% noise added into the data.

Figure 4 presents a comparison of the inversion results in Example 2. The three priors follow the true slope well on the two piecewise-linear segments, and the errors are mainly near the kink and at the endpoints. Among them, the Gaussian prior shows the most obvious bias and underestimates the value at the kink compared with the ground truth; the TV–Gaussian produces smoothing bias near the sharp kink; the PH–Gaussian agrees best with the ground truth in both peak height and kink location, largely removing over-smoothing and showing a higher fit on the rising and falling segments. This indicates that the introduced topological information helps reduce peak bias and improve shape fidelity.

Table 2: Numerical results of Example 2 with different noise levels

$\epsilon$	Gaussian Prior		TV-Gaussian Prior		PH-Gaussian Prior	
	$\hat{\lambda}$	$e_r$	$\hat{\lambda}$	$e_r$	$\hat{\lambda}$	$e_r$
0.01	/	0.0857	26.34	0.0345	8.82	0.0248
0.03	/	0.1292	29.75	0.0668	9.79	0.0529
0.05	/	0.1630	33.78	0.1163	10.29	0.0673

Figure 5 shows, for Example 2 with 1% noise, the posterior density of the regularization parameter  $\lambda$  under the TV Gaussian and PH Gaussian priors. Figure 6 presents the 95% credible interval obtained with the PH Gaussian prior; the posterior conditional mean  $\gamma$  agrees very well with the exact solution. Table 2 indicates that the TV Gaussian prior outperforms the Gaussian prior, and the PH Gaussian prior attains a slightly lower error than the TV Gaussian prior.

Example 3. The conductivity  $\alpha(x)$  is set as  $\alpha(x) = e^x$ , and the exact Robin coefficient  $\gamma^\dagger(t)$  is given by  $\gamma^\dagger(t) = \frac{1}{2}\chi_{\{\frac{3}{10} \leq t \leq \frac{7}{10}\}}$ . The boundary conditions, source term, and initial condition are specified such that the analytical solution to the direct problem (1) is given by  $u(x, t) = (x^2 + 1) \sin(\pi t)$ .

In this example, the different priors proposed in Section 3 are also tested. The parameters for these priors are set as follows: for  $C_0^{\text{exp}}$ ,  $l = 0.03$ ,  $\lambda = 0.1$ ; for the topological prior formulation,  $\theta = 3$ ,  $\beta = 0.001$ . The numerical results for Example 3 with 1% and 5% noise in the data are shown in Figure 7:

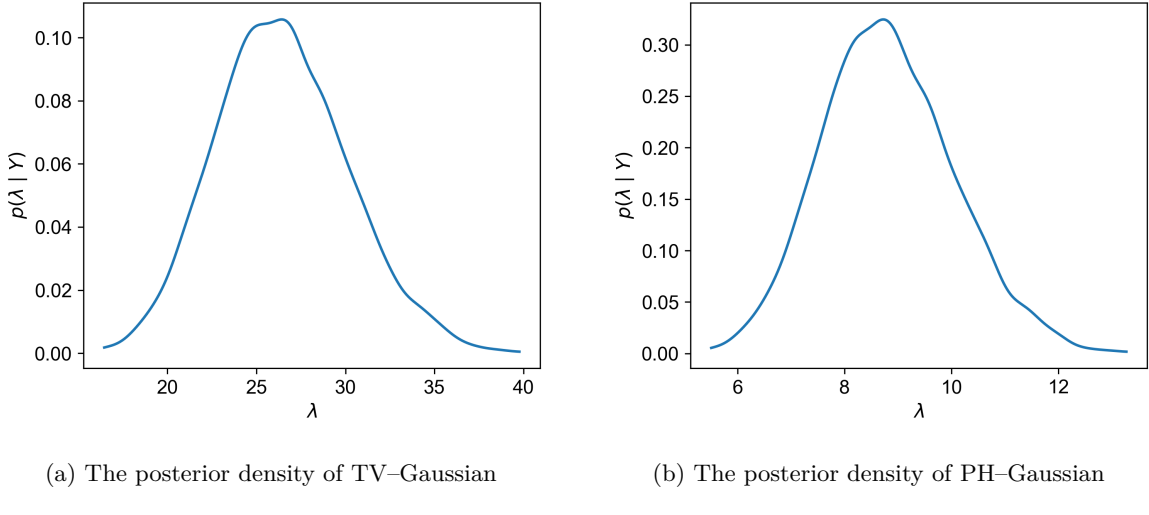


Figure 5: The posterior density of the scaling parameter  $\lambda$  for Example 2 with 1% noise added into the data.

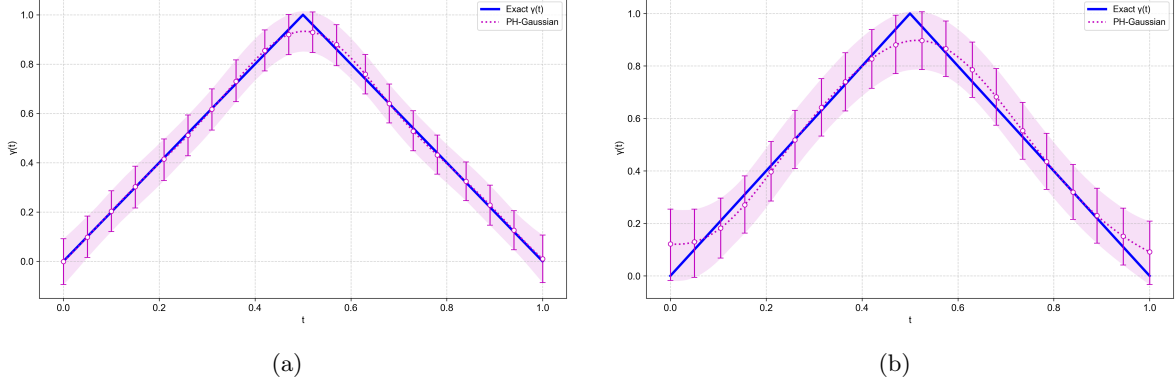


Figure 6: The numerical results for Example 2 with (a) 1% and (b) 5% noise added into the data.

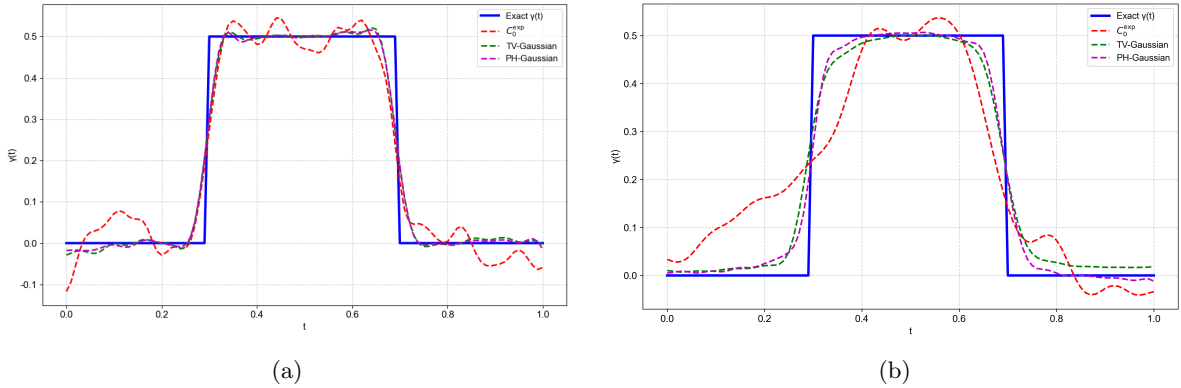


Figure 7: The numerical results for Example 3 with (a) 1% and (b) 5% noise added into the data.

As shown in Figure 7, the Gaussian prior method shows clear oscillations and cannot effectively reduce noise. The TV–Gaussian prior incorporates a total variation regularization term, which suppresses oscillations and yields smoother reconstructions. The PH–Gaussian prior also benefits from regularization, but additionally preserves global structures and sharp discontinuities more effectively. It remains robust even under higher noise levels (e.g., 5%), and reconstructs the overall shape more accurately than the TV–Gaussian prior.

Table 3: Numerical results of Example 3 with different noise levels

$\epsilon$	Gaussian Prior		TV-Gaussian Prior		PH-Gaussian Prior	
	$\hat{\lambda}$	$e_r$	$\hat{\lambda}$	$e_r$	$\hat{\lambda}$	$e_r$
0.01	/	0.1987	136.46	0.1487	50.05	0.1432
0.03	/	0.3076	162.39	0.1874	55.33	0.1667
0.05	/	0.3611	174.06	0.2086	58.15	0.1849

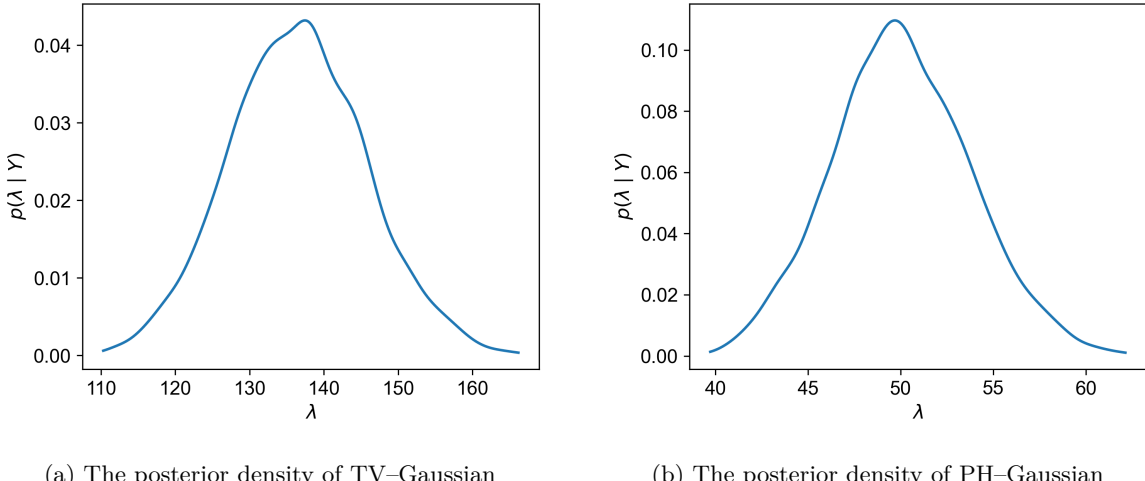


Figure 8: The posterior density of the scaling parameter  $\lambda$  for Example 3 with 1% noise added into the data.

Figure 8 illustrates the posterior densities of the regularization parameter  $\lambda$  for Example 3 under 1% noise: the posterior conditional mean for TV–Gaussian is 136.46, while that for PH–Gaussian is 50.05, as shown in Table 3. The numerical results indicate that the automatically determined regularization parameter  $\lambda$  is quite optimal. For the case with 1% and 5% noise in Example 3, Figure 9 presents the 95% credible intervals based on PH–Gaussian. It can be observed that the posterior conditional mean  $\gamma$  is in excellent agreement with the exact solution.

## 4 Conclusions

In this paper, we studied the identification of a time-dependent Robin coefficient in a parabolic heat-transfer problem within a Bayesian framework. A PH–Gaussian prior was adopted to incorporate topological information of the Robin coefficient, and a hierarchical Bayesian method was used to infer the regularization parameter  $\lambda$ . Numerical results show that the PH–Gaussian prior performs well. Also, the hierarchical Bayesian framework can automatically determine suitable regularization parameters. The proposed method offers a novel approach to solving the Robin coefficient identification problem in inverse heat conduction equations.

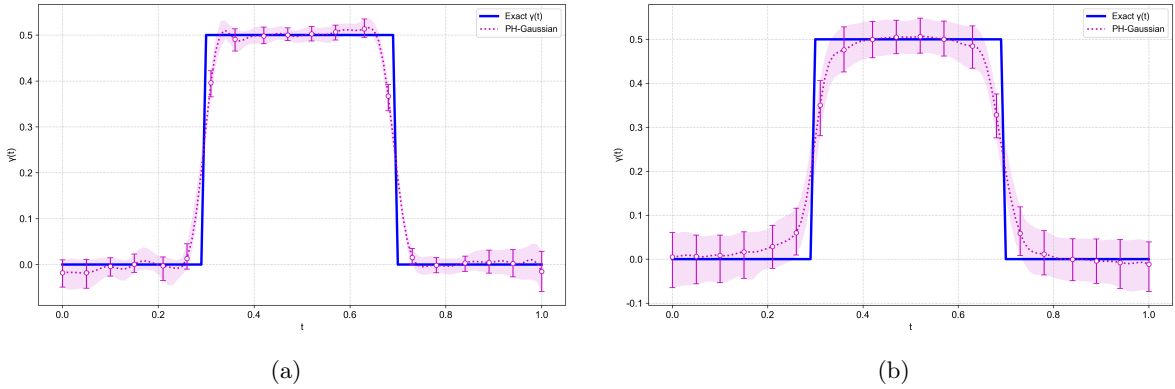


Figure 9: The numerical results for Example 3 with (a) 1% and (b) 5% noise added into the data.

## References

- [1] Bangti Jin and Jun Zou. Numerical estimation of piecewise constant robin coefficient. *SIAM journal on control and optimization*, 48(3):1977–2002, 2009.
- [2] Gabriele Inglese. An inverse problem in corrosion detection. *Inverse problems*, 13(4):977, 1997.
- [3] Giovanni Alessandrini, L Del Piero, Luca Rondi, et al. Stable determination of corrosion by a single electrostatic boundary measurement. *Inverse problems*, 19(4):973–984, 2003.
- [4] Robert J Arthern and G Hilmar Gudmundsson. Initialization of ice-sheet forecasts viewed as an inverse robin problem. *Journal of Glaciology*, 56(197):527–533, 2010.
- [5] Mourad Choulli. On the determination of an unknown boundary function in a parabolic equation. *Inverse problems*, 15(3):659, 1999.
- [6] Mourad Bellouquied, Jin Cheng, and Mourad Choulli. Stability estimate for an inverse boundary coefficient problem in thermal imaging. *Journal of mathematical analysis and applications*, 343(1):328–336, 2008.
- [7] Abdollah Shidfar, R Pourgholi, and M Ebrahimi. A numerical method for solving of a nonlinear inverse diffusion problem. *Computers & Mathematics with Applications*, 52(6-7):1021–1030, 2006.
- [8] Marián Slodicka and Roger Van Keer. Determination of a robin coefficient in semilinear parabolic problems by means of boundary measurements. *Inverse Problems*, 18(1):139, 2002.
- [9] M Slodička, D Lesnic, and TTM Onyango. Determination of a time-dependent heat transfer coefficient in a nonlinear inverse heat conduction problem. *Inverse Problems in Science and Engineering*, 18(1):65–81, 2010.
- [10] Markus Biegert and Mahamadi Warma. The heat equation with nonlinear generalized robin boundary conditions. *Journal of Differential Equations*, 247(7):1949–1979, 2009.
- [11] Bangti Jin and Xiliang Lu. Numerical identification of a robin coefficient in parabolic problems. *Mathematics of Computation*, 81(279):1369–1398, 2012.
- [12] TTM Onyango, Derek B Ingham, and Daniel Lesnic. Inverse reconstruction of boundary condition coefficients in one-dimensional transient heat conduction. *Applied mathematics and computation*, 207(2):569–575, 2009.
- [13] Fenglian Yang, Liang Yan, and Ting Wei. The identification of a robin coefficient by a conjugate gradient method. *International journal for numerical methods in engineering*, 78(7):800–816, 2009.
- [14] Weifu Fang and Suxing Zeng. A direct solution of the robin inverse problem. *The Journal of Integral Equations and Applications*, pages 545–557, 2009.

---

- [15] WB da Silva, JCS Dutra, CEP Kopperschmidt, D Lesnic, and RG Aykroyd. Sequential estimation of the time-dependent heat transfer coefficient using the method of fundamental solutions and particle filters. *Inverse Problems in Science and Engineering*, 29(13):3322–3341, 2021.
- [16] Bangti Jin. Fast bayesian approach for parameter estimation. *International Journal for Numerical Methods in Engineering*, 76(2):230–252, 2008.
- [17] Liang Yan, Fenglian Yang, and Chuli Fu. A bayesian inference approach to identify a robin coefficient in one-dimensional parabolic problems. *Journal of Computational and Applied Mathematics*, 231(2):840–850, 2009.
- [18] Bangti Jin and Jun Zou. A bayesian inference approach to the ill-posed cauchy problem of steady-state heat conduction. *International journal for numerical methods in engineering*, 76(4):521–544, 2008.
- [19] Chengxin Shi and Hao Cheng. Identify the robin coefficient in an inhomogeneous time-fractional diffusion-wave equation. *Journal of Computational and Applied Mathematics*, 434:115337, 2023.
- [20] Aksel K Rasmussen, Fanny Seizilles, Mark Girolami, and Ieva Kazlauskaitė. The bayesian approach to inverse robin problems. *SIAM/ASA Journal on Uncertainty Quantification*, 12(3):1050–1084, 2024.
- [21] Zhewei Yao, Zixi Hu, and Jinglai Li. A tv-gaussian prior for infinite-dimensional bayesian inverse problems and its numerical implementations. *Inverse Problems*, 32(7):075006, 2016.
- [22] Zhiliang Deng, Haiyang Liu, Xiaofei Guan, Zhiyuan Wang, and Xiaomei Yang. A persistent-homology-based bayesian prior for potential coefficient reconstruction in an elliptic partial differential equation. 2025.